DALTON
FULL PAPER

Manipulating the properties of MLCT excited states †

Peter A. Anderson,[a] F. Richard Keene,*[a] Thomas J. Meyer,*‡[b] John A. Moss,[b] Geoffrey F. Strouse[b] and Joseph A. Treadway[b]

[a] *School of Pharmacy & Molecular Sciences, James Cook University, Townsville, Queensland 4811, Australia*
[b] *Department of Chemistry, University of North Carolina CB#3290, Chapel Hill, NC 27599-3290, USA*

Received 2nd July 2002, Accepted 9th August 2002
First published as an Advance Article on the web 18th September 2002

Systematic variation of the ligand environment has allowed design of the absorbance characteristics of polypyridyl complexes of ruthenium(II) to produce "black absorbers" which absorb throughout the visible region. The presence of acceptor ligands with low-lying π* levels red shift the energies of the lowest energy MLCT bands, while MLCT and π ⟶ π* bands originating on other ligands can be used to fill in the higher-energy regions of the spectrum. Incorporation of anionic ligands or other electron-donating ligands causes a red shift in MLCT band energies compared to bpy by manipulation of dπ energy levels. Attention to these design principles has led to the synthesis of complexes which absorb appreciably in the near IR, and are free from complications caused by thermally accessible dd states. Although their emission energies (and energy gaps) are at low energy in the near IR, the use of lowest lying, delocalised acceptor ligands provides lifetime enhancements (compared to bpy) that can be dramatic.

Introduction

Polypyridyl complexes of d^6 metal ions such as Ru^{II}, Os^{II} and Re^{I} have been used extensively as photosensitisers for studies of photo-induced electron and energy transfer in molecular assemblies[1–22] and surface sensitisation of colloidal TiO_2.[23–30] This interest arises because of their useful absorbance and emission characteristics, their chemical stabilities, and their low barriers to electron and energy transfer. UV light absorption by these complexes is dominated by intense ligand-centred π ⟶ π* bands, and in the visible region by metal-to-ligand charge-transfer (MLCT) bands.[31–35]

Although the synthetic chemistry of these complexes is well established and much is known about their spectral and photophysical characteristics, there remain outstanding issues in their exploitation. In general, the Re^{I} complexes studied have been based on the *fac*-$Re^{I}(CO)_3$ core,[36–38] which imposes limitations on variation in ligand environment and stereochemistry. In addition, these complexes typically absorb appreciably only in the UV and high-energy regions of the spectrum because of the effect of the carbonyl ligands on the energy of the dπ(Re) orbitals. This results in greatly lowered visible absorptivity and highly convoluted electronic spectra.

Polypyridyl osmium(II) complexes have more desirable spectral properties, including MLCT absorptions at lower energy and contributions to the spectra from direct ground state to ^{3}MLCT absorptions at lower energy. The substitutional inertness of Os^{II} compounds does impose some synthetic restrictions.[34,35,39] Further, from the photophysical point of view, at the same energy gap, Os^{II} complexes tend to have significantly shorter lifetimes than their Ru^{II} analogues. This is because enhanced spin–orbit coupling at the $d\pi^5(Os^{III})$ core increases the singlet character in the lowest-lying MLCT excited state, increasing excited-state/ground-state mixing.[31,32]

Polypyridyl ruthenium(II) complexes exhibit desirable light absorption in the visible spectral region, and there is a well-developed synthetic chemistry for the preparation of an extensive range of complexes.[40–46] Recent advances in separations and stereochemical synthesis have extended the structural versatility of the complexes far beyond that of the *fac*-$Re^{I}(CO)_3$ and Os^{II} cores.[47] Complications remain from low-lying, metal-centred dd excited states. They are typically populated by thermally activated barrier crossing following MLCT excitation. Their population leads to shortened lifetimes and net ligand-loss photochemistry.[48–61] Such problems do not exist with Os^{II} and Re^{I} complexes since the ligand field splitting energy, 10Dq, is approximately 30% higher for the third transition series compared to the second which increases the MLCT–dd energy gap.[62] The Ru^{II} complexes are typically visible absorbers but at higher energy than the equivalent Os^{II} complexes.

In Ru^{II} and Os^{II} complexes of this type, ligand substitution can be used to vary the spectral properties of the complexes systematically.[35,39,44,45,63,64] For example, lowering the π* level of an acceptor ligand by incorporation of an electron-withdrawing substituent can red-shift the lowest-energy MLCT absorption. However, the resulting decrease in the ground-to-excited state energy gap leads to a concomitant shortening of the excited state lifetime. This effect is described quantitatively by the energy gap law.[65–70] It predicts that, in the absence of competing nonradiative events, the nonradiative lifetime should vary exponentially with the energy gap for a common acceptor ligand.[65,71–73]

The first goal of this study was to systematically manipulate ligand properties in Ru^{II}-based chromophores in order to maximise π ⟶ π* and MLCT absorptivity throughout the UV/visible spectral region. This is an important requirement for an efficient light-to-chemical conversion system, and has been emphasised by the work of Bignozzi,[29,74,75] Grätzel, and others[76–82] in their attempts to prepare practical solar energy devices using Ru^{II} dye-derivatised nanocrystalline TiO_2 substrates.

† Electronic supplementary information (ESI) available: absorbance spectrum for $[Ru(Me_2bpy)\{bpy(CO_2Et)_2\}(Et_2dtc)]^+$ with band assignments; emission spectra for $[Ru(Me_2bpy)(Me_4bpy)(BL)]^{2+}$ (BL = dpq or dpp); results of temperature dependent luminescence measurements on $[Ru(bpy)_2(dpp)](PF_6)_2$. See http://www.rsc.org/suppdata/dt/b2/b206375a/

‡ Present address: Los Alamos National Laboratory, MS A127, Los Alamos, NM 87545, USA.

 DOI: 10.1039/b206375a

The second goal of the study was to overcome the limitation on excited-state lifetimes imposed by the energy gap law. It follows that black chromophores will have small energy gaps and consequently could have extremely short lifetimes. This would decrease their applicability in studies of excited-state dynamics, in assays based on emission anisotropy, or as sensitisers.

The third goal was to minimise complications from dd state deactivation and ligand loss population of these states shortens lifetimes and can lead to photodecomposition.[48,49,53,54]

A series of observations from previous work led to the synthetic strategy employed. The first was based on the electronic character of the excited state and the associated $^1(d\pi–\pi^{*0}) \longrightarrow {}^1(d\pi–\pi^{*1})$ ground-to-excited state transition illustrated below for $[Ru(bpy)_3]^{2+}$ {bpy = 2,2′-bipyridine}.

$$[Ru^{II}(bpy)_3]^{2+} \xrightarrow{h\nu} [Ru^{III}(bpy)_2(bpy^{\bullet-})]^{2+*}$$

Strategies have been developed to red-shift absorbances in tris(heteroleptic)ruthenium(II) complexes,[44,63] for example by lowering the π* energy level of a ligand by the use of electron-withdrawing substituents, the use of electron-rich (*e.g.* anionic) ligands to stablise the hole at Ru^{III} in the MLCT excited state, or a combination of the two.

The second was that MLCT transitions occur to each ligand in a mixed chelate complex.[31,83,84] This means that acceptor ligands other than the final acceptor ligand can be chosen to fill in the higher energy region of the spectrum, with the lowest energy acceptor used to extend the absorbance to lower energies. In addition, ligand-centred $\pi \longrightarrow \pi_1^*$ and $\pi \longrightarrow \pi_2^*$ absorptions appear in the UV;[85] MLCT transitions to higher-lying π* orbitals ($d\pi \longrightarrow \pi_2^*$) add absorptivity to the high-energy visible region and UV. A preliminary account of this design strategy has been published previously.[63]

The third observation was that following MLCT excitation of heteroleptic complexes, the excited electron ultimately resides on the ligand having the lowest-energy π* orbital,[86–93] and nonradiative lifetimes can be controlled by controlling its structure. The key to the energy gap law is the role that the energy gap plays in dictating the extent of ground-excited state vibrational overlap. This is the overlap in vibrational modes that are coupled to the nonradiative transition. On a mode-for-mode basis, the magnitude of these overlaps depend on the energy gap and the changes in equilibrium displacement which when summed, provide a measure of excited state distortion.[65,94]

The vibrational modes that dominate deactivation of MLCT excited states are primarily ring stretching and bending modes on the polypyridyl acceptor ligand.[95–97] In MLCT excited states, electron occupation of the lowest π* acceptor orbital results in increases in average C–C and C–N bond lengths in the acceptor ligand.[97] This distortion can be decreased (compared to bpy) by using a rigid skeletal σ-bonding framework and/or an extended delocalised π* acceptor orbital. In the latter case, the changes in average displacements are decreased and the overlaps scale as the square of the displacements. The appearance of the effect would be expected in complexes containing the delocalised ligand dpb (Fig. 1) compared with complexes incorporating bpy as the acceptor.

A fourth observation deals with metal-centred dd states. It has been noted in the literature that decreasing the local electronic symmetry at Ru^{II} decreases dd excited state participation by increasing the activation barrier to these states.[98] Use of delocalised acceptor ligands comparable in σ-donating ability to bpy but with low lying π* acceptor levels also provides a useful means for increasing the barrier to MLCT to dd conversion.

In a final section, application of these ideas to the preparation of dyes for sensitisation of TiO_2 solar cells is described.

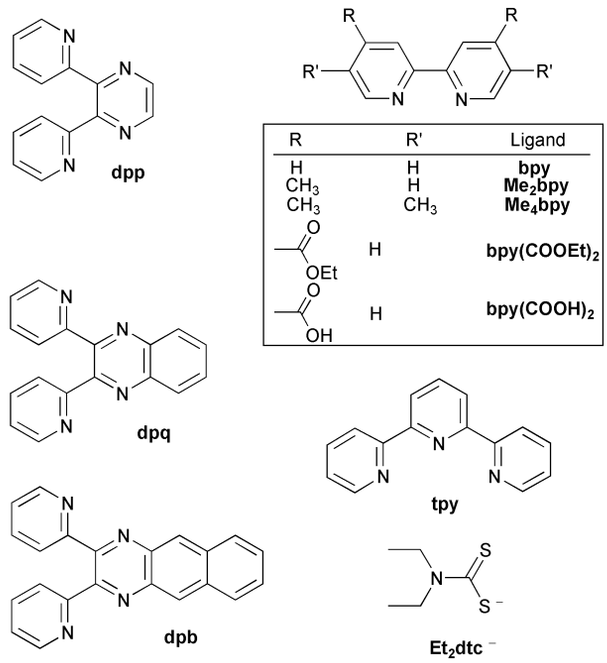

Fig. 1 Some ligands used in the preparation of black chromophores: dpp = 2,3-bis(2-pyridyl)pyrazine; dpq = 2,3-bis(2-pyridyl)quinoxaline; dpb = 2,3-bis(2-pyridyl)benzoquinoxaline; bpy = 2,2′-bipyridine; Me_2-bpy = 4,4′-dimethyl-2,2′-bipyridine; Me_4bpy = 4,4′,5,5′-tetramethyl-2,2′-bipyridine; bpy$(CO_2Et)_2$ = diethyl 2,2′-bipyridine-4,4′-dicarboxylate; bpy$(CO_2H)_2$ = 2,2′-bipyridine-4,4′-dicarboxylic acid; Et_2dtc^- = diethyl dithiocarbamate anion; tpy = 2,2′:6′,2″-terpyridine.

A great deal of activity has occurred in recent years in the use of polypyridyl complexes of ruthenium(II) as photosensitisers of nanocrystalline TiO_2.[25–27,30,74,77,78,99,100] Following the absorption of visible light, electron transfer from the dye to the conduction band of the TiO_2 can lead to efficient and permanent separation of oxidative and reductive redox equivalents. Monochromatic light-to-chemical conversion efficiencies approaching unity have been obtained.[28,79] White light conversion efficiencies are far lower because of the absence of dyes which absorb strongly throughout the visible. An exception is a report by Nazeeruddin *et al.*[24] on sensitisation by $\{(C_2H_5)_4N\}[Ru(tct)(SCN)_3]$ (tct is a triply-carboxylated terpyridine) for which efficient charge injection was observed throughout much of the visible.

Experimental

Physical methods

UV-Visible spectra were recorded on a Hewlett-Packard 8452A diode array or Cary 14 spectrophotometer. The Cary 14 was interfaced to an IBM PC by OnLine Systems, Inc. ^1H NMR spectra were recorded on BRUKER AM300 or WM250 spectrometers. Current measurements on photo-electrochemical experiments were made by using a Keithley Electrometer, Model 6512. Photolyses in these experiments were carried out by using a 150 W mercury lamp equipped with a 480 nm low-pass filter and a water cell used as an infrared filter. Light from the lamp was focussed by using two glass lenses so that the entire electrode surface was irradiated.

Electochemical measurements were made in a dry box (N_2) by using an EG&G PAR Model 273 potentiostat or a BAS 100A Electrochemical Analyser. Cyclic voltammetry was carried out in a standard three-compartment cell with a 4 mm platinum disc working electrode, a platinum wire counter electrode, and a $Ag/AgNO_3$ {0.01 M $AgNO_3$/0.1 M tetra-*n*-butylammonium hexafluorophosphate (TBAH) in acetonitrile} reference electrode, which was regularly standardised against a

saturated sodium chloride calomel electrode (SSCE). Regardless of the cell arrangement, all potentials are quoted relative to the SSCE.

All metal complexes were purified by cation-exchange HPLC on a Brownnlee CX-300 Prep 10 column or an Alltech HEMA-IEC BIO SB1000 column (3 and 1.5 mL min^{-1} respectively) with linear gradient elution with 0–400 mM KBr in 2 : 3 (v/v) CH_3CN–aqueous phosphate buffer (0.6 mM; pH = 7.2). The elutions were controlled by a Rainin Dynamax SD-300 solvent delivery system equipped with 25 mL min^{-1} pump heads and monitored at a Shimadzu SPD-M10AV diode-array UV-visible spectrometer fitted with a 4.5 mm path length flow cell. The compounds were isolated from the eluent as hexafluorophosphate salts by addition of saturated KPF_6 solution followed by slow removal of the acetonitrile at room temperature in the dark under vacuum. The resulting precipitates were collected by vacuum filtration.

Absorption spectra of derivatised TiO_2 films were obtained in air with the electrodes wet with acetonitrile or ethanol. The absorbance spectrum of an underivatised TiO_2 electrode was subtracted from the spectrum of each sample, and the resulting spectrum normalised to zero absorbance in the flat background region from 700–800 nm. The percentage of light absorbed by the chromophores is expressed as the light-absorbing efficiency (and the relationship $LHE = 1–10^{-Absorbance}$).

Photocurrent measurements were carried out in a two-electrode sandwich-type cell. The counter electrode was a Pt foil sealed in a block of epoxide resin (Bueler) to form the cell base. The TiO_2 electrode was sandwiched against the counter electrode with a parafilm (AlCan) spacer and an electrolyte solution containing 0.5 M NaI and 0.05 M I_2 in propylene carbonate. The irradiation source was a 75 W xenon lamp powered by a high precision constant current source coupled to a *f*/4 matched monochromator with 1200 lines/in grating blazened at 500 nm. Incident light intensity was measured with a single crystal photocell (Radio Shack 277–1201) calibrated with a standard detector (UDT Instruments, Model S370 optometer). Incident photo-to-current conversion efficiency (IPCE) at each incident radiation wavelength was calculated as $IPCE\ (\lambda) = \{(1240\ eV\ nm)I_{ph}\}/\lambda P_0$. In this expression, I_{ph} is the photocurrent density in μA cm^{-2}, λ is the wavelength of incident radiation in nm, and P_0 is the photon flux in μW cm^{-2}. Calculated IPCE values at each λ were corrected for losses due to light absorption and reflection off the glass support.

Corrected emission spectra for complexes emitting in the visible region of the spectrum were recorded on a Spex Fluorolog-2 emission spectrometer equipped with a 450 W Xe lamp and a cooled ten-stage Hamamatsu R928 or R664 photomultiplier. The optical responses for each set-up were corrected with a calibration curve generated with 1.0 mm slits by using a NIST calibrated standard lamp (Optronics Laboratories, Inc. Model 22M), controlled with a precision current source at 6.50 W (Optronics Laboratories, Inc. Model 65). The manufacturer's recommendations regarding lamp geometry were followed. Unless otherwise noted, all spectra were obtained in CH_3CN solutions at room temperature in 1 cm path length quartz cells (OD < 0.5) with right angle observation of the emitted light.

For complexes emitting predominantly in the near IR region (emission maxima > 850 nm), corrected emission spectra were obtained by using a chopped (81 Hz) Ar^+ ion laser (514 nm, 500 mW) as an excitation source. Emitted light was collected with *f*-matched collection optics into a 1 metre Spex monochromator (3.0 mm slits, 100 nm blaze, 1200 grooves mm^{-1}) coupled to a one-stage cooled indium–gallium–arsenide (InGaAs) detector. Luminescence traces were collected as difference spectra (light on minus light off) by using a PAR lock-in amplifier (1 s average, 200 μV scale). Corrections for detector response, grating and monochromator anomalies were effected with a standard tungsten filament lamp.

Time-resolved emission measurements were made by using a PRA LN 1000/LN102 nitrogen laser/dye laser combination equipped with Coumarin 460 dye for sample excitation. Emission intensity was monitored at a right angle to the excitation source with a PRA monochromator, model B204-3, set at the emission maximum and a Hamamatsu R-928 phototube. Transient absorbance difference spectra were measured by using an apparatus described previously.[20,101,102] A PDL-2 pulsed dye laser (Coumarin 460 dye) pumped by the third harmonic (354.7 nm) of a Quanta-Ray DCR-2A Nd-YAG laser was used as an excitation source providing an ~5 ns pulse with 2.5–3.5 mJ $pulse^{-1}$. An Applied Photophysics laser kinetic spectrometer (consisting of a 300 W pulsed Xe lamp source, a *f*/3.4 grating monochromator, and a five-stage photomultiplier tube) was employed as a detection system. For both experiments, decay traces were recorded on a Lecroy 7200A digital oscilloscope interfaced to an IBM PC. Samples were dissolved in CH_3CN (OD < 0.3) and freeze–pump–thaw degassed (4×, 10^{-5} mm Hg) prior to measurement. The digitised traces were fitted to the appropriate model with a Levenberg–Marquardt routine.[103]

Temperature-dependent luminescence and transient absorbance measurements were carried out in a liquid nitrogen-cooled Oxford Instruments vacuum cryostat modified for use with small (~1 mL) sample volumes to ensure rapid temperature equilibration and to minimise temperature gradients. Each temperature was maintained with a combination of variable He carrier gas flow and a heater controlled by an Oxford Instruments 3120 temperature controller. Temperatures accurate to ±0.2 °C were measured with a thermocouple attached to the sample <2 mm from the interrogation path by using an Omega HH-51 digital thermometer. Data were acquired only after each temperature had been maintained for at least 20 min.

Photochemical quantum yields were measured by utilising an apparatus of our own design. Samples were prepared by dissolving sufficient material in dichloromethane to achieve an optical density at the irradiation wavelength (typically 460 nm) of 1.0 in a 1 cm cell. Tetra-*n*-butylammonium chloride was added in a 100-fold excess and the samples sparged with dichloromethane-saturated oxygen-scrubbed argon for 1 h. The samples were irradiated with monochromatic light generated by an XBO 75W/2 model collimated 75 W Xe lamp powered by a high precision constant current source (PTI-LPS-220) operating at 5.4 amps. After passing through a PTI-A-1010 *f*/4 matched monochromator with 1200 lines mm^{-1} grating blazed at 500 nm, the light was collected and focussed by using glass lenses to a point ~1 cm into the sample cell. During the photolyses, the sample was stirred continuously and thermostatted in a compartment with a 12 cm path length. At regular intervals, the sample was removed from the irradiation beam and shaken. The photolysis cell was designed so that an aliquot of the photolysate could be poured through an arm into a 1 cm cell without exposing the sample to air. The absorbance spectrum was measured and the cell tilted to allow the aliquot to flow back into the photolysis path. Calculation of the quantum yields could therefore be carried out with the assumption that all of the impinging light was absorbed in the large path length cell since the optical density was >10, Beer's law was obeyed in the small path length cell since the optical density was below 1, and the photo-products absorbed none on the light since less than the first 1% of the reaction was followed. The light intensity was measured by utilizing Reineckate salt as an actinometer.[104]

Materials

Hydrated $RuCl_3 \cdot 3H_2O$ (Strem or Aldrich), 2,3-bis(2-pyridyl)-pyrazine (dpp; Aldrich 98%), formic acid (BDH AnalAR 90% or Fisher Certified 88%) 4,4′-dimethyl-2,2′-bipyridine (Me_2bpy; Aldrich), potassium thiocyanate (Aldrich), 1,2-dimethoxy-

ethane (Fluka puriss or Aldrich anhydrous 99.5%), 2-methoxyethanol (Aldrich 99.3%), titanium isopropoxide (Aldrich) and polyethylene glycol {Aldrich, average M_n *ca.* 2000 (Carbowax™)} were used as supplied. Trifluoromethanesulfonic acid (Fluka purum or 3M) and propylene carbonate (Aldrich) were freshly vacuum distilled prior to use. Trimethylamine *N*-oxide (TMNO) was obtained by vacuum sublimation of the hydrate (Fluka purum) at 120 °C. Potassium diethyldithiocarbamate was obtained from sodium diethyldithiocarbamate trihydrate (Aldrich) by a cation exchange procedure. Tetra-*n*-butylammonium hexafluorophosphate (TBAH; Aldrich) was recrystallised twice from ethanol–water and dried at 60 °C under vacuum prior to use. Spectral grade acetonitrile (Burdick and Jackson), methanol (Burdick and Jackson), and ethanol (freshly distilled over Mg/I_2) were used for all spectroscopic and electrochemical measurements.

Preparation of TiO_2 electrodes

Tin-doped indium oxide electrodes modified with high-surface area titanium dioxide were prepared by using a modification of the previously published method.[79] Titanium isopropoxide (25 mL) was added dropwise with stirring to distilled water (~150 mL) containing 70% HNO_3 (1.05 mL). The sol was heated with stirring in an open round-bottom flask at 85 °C until the solution volume was 50 mL (135 g TiO_2 per L). The resulting sol was autoclaved by sealing the TiO_2 (~35 mL) in a 12.5 × 4 cm glass vessel and heating in an oven at 200 °C for ~14 h, inducing precipitation of the TiO_2. After cooling, the glass was opened and 40% w/w polyethylene glycol (Carbowax) was added to the stirring TiO_2 suspension. The suspension was stirred overnight to give a mixture which was fairly viscous and difficult-to-spread.

Tin(IV)-doped indium oxide (ITO) electrodes (Delta Technologies, 20 Ω cm^{-2}) were cleaned by sonicating for 15 min in 1 : 1 : 5 NH_4OH–H_2O_2–H_2O and rinsing with water and ethanol. A 75 × 50 mm ITO sheet was masked by placing two pieces of Scotch tape lengthwise on the surface, leaving an area 1 cm wide exposed between them. Several drops of the TiO_2 mixture were placed at one end of the electrode and spread evenly across the exposed area with a test tube in one sweep. The TiO_2 film was allowed to dry in air for 30 min, the electrode cut into ~7 × 50 mm pieces, and heated in a Lindberg furnace at 400 °C under O_2 for 30 min.

The electrodes were derivatised by soaking for 12–24 h in ethanol or acetonitrile solutions containing ~1 mM Ru complex. Immediately prior to introduction to the dye solution, electrodes were heated to 400 °C under O_2 for 15 min to remove adsorbed water. The electrodes were cooled to approximately 80 °C and placed in the dye solution while still warm. After derivatisation, TiO_2 electrodes were stored in acetonitrile or ethanol until use.

Syntheses

Chemical analyses were performed by Oneida Research Services, Inc. (Whitesboro, NY, USA) or the Chemical & Microanalytical Services Pty. Ltd. (Melbourne, Australia). $[Ru(bpy)_3](PF_6)_2$[45] and the ligands dpq and dpb[105] (Fig. 1) were prepared according to literature procedures. The ligands $bpy(CO_2Et)_2$,[106,107] $bpy(CO_2H)_2$[107] and Me_4bpy[108] were prepared as described previously. The complexes $[Ru(CO)_2Cl_2]_n$, $[Ru\{bpy(CO_2Et)_2\}(CO)_2(CF_3SO_3)_2]$, $[Ru(Me_2bpy)(Me_4bpy)(CO)_2](PF_6)_2$, $[Ru(Me_2bpy)\{bpy(CO_2Et)_2\}(CO)_2](PF_6)_2$, $[Ru(Me_2bpy)(Me_4bpy)(dpp)](PF_6)_2$ and $[Ru(Me_2bpy)\{bpy(CO_2Et)_2\}(dpp)](PF_6)_2$ were prepared as described previously.[44]

$[Ru\{bpy(CO_2Et)_2\}(dpb)(CO)_2](PF_6)_2$. $[Ru\{bpy(CO_2Et)_2\}(CO)_2(CF_3SO_3)_2]$ (120 mg, 0.16 mmol) and dpb (110 mg, 0.33 mmol) were added to 95% ethanol (150 mL) and the suspension deaerated with Ar for 45 min. The solids dissolved upon heating the mixture and the resulting solution was allowed to heat at reflux under an Ar atmosphere for 3 h. The mixture was cooled to room temperature and the solvent removed under reduced pressure. Boiling water (125 mL) was added to the resulting grey residue and the mixture hot-filtered and allowed to cool. Addition of a saturated solution of NH_4PF_6 (5 mL) resulted in the precipitation of the pale orange crude product, which was twice recrystallised from ethanol–acetone. Yield: 55 mg (33%).

$[Ru(Me_2bpy)\{bpy(CO_2Et)_2\}(dpq)](PF_6)_2\cdot 0.25HPF_6$. A suspension of dpq (31 mg, 0.22 mmol) and $[Ru(Me_2bpy)\{bpy(CO_2Et)_2\}(CO)_2](PF_6)_2$ (51 mg, 0.055 mmol) in 1,2-dimethoxyethane (15 mL) was sparged with oxygen-scrubbed Ar for 45 min. The mixture was heated to reflux under an Ar atmosphere resulting in a change from colourless to pale orange. Over the course of 30 min, TMNO (12 mg, 0.16 mmol) dissolved in similarly sparged 1,2-dimethoxyethane (15 mL) was added dropwise *via* an addition funnel equipped with a pressure-equalisation arm. The dark red solution was heated at reflux for an additional 3 h, cooled to room temperature, and evaporated to dryness under reduced pressure. The residue was dissolved in a minimum volume of acetone, filtered to remove unreacted TMNO, and rapidly diluted with de-ionized water (~1 L). This solution was absorbed onto a column of CM Sephadex C-25 cation exchanger, and eluted with a 0–400 mM KNO_3 salt gradient. An initial yellow band eluting at low ionic strength as well as the leading edge of a second red band were discarded. The remainder of the second band was collected. A fine precipitate appeared upon addition of saturated aqueous solution KPF_6 (~2 mL). Extraction with dichloromethane (3 × 50 mL) removed nearly all colour from the aqueous layer. The organic layers were combined, dried, and concentrated under vacuum to ~5 mL. Slow addition of this solution to diethyl ether (100 mL) produced a flocculent precipitate which was collected, washed with water (5 × 5 mL) and diethyl ether (5 × 5 mL), and allowed to dry overnight under vacuum at 60 °C. Yield: 32 mg (50%). Anal. calculated for $C_{46}H_{40.25}N_8F_{13.5}O_2P_{2.25}Ru$: C, 46.2; H, 3.39; N, 9.4. Found: C, 46.5; H, 3.65; N, 8.9%.

$[Ru(Me_2bpy)\{bpy(CO_2Et)_2\}(dpb)](PF_6)_2\cdot 0.33HPF_6$. The compound was prepared in a manner analogous to $[Ru(Me_2bpy)\{bpy(CO_2Et)_2\}(dpq)](PF_6)_2\cdot 0.25HPF_6$. $[Ru(Me_2bpy)\{bpy(CO_2Et)_2\}(CO)_2](PF_6)_2$ (65 mg, 0.070 mmol) was reacted with TMNO (16 mg, 21 mmol) in the presence of dpb (47 mg, 0.14 mmol). Yield: 57 mg (67%). ^1H NMR (acetone-d_6): δ 1.42 (t), 1.45 (t), 2.43 (s), 2.54 (s), 4.44 (m), 7.40 (m), 7.65 (m), 7.90 (m), 8.32 (m), 8.75 (s), 8.88 (s), 9.48 (s). Anal. calculated for $C_{50}H_{42.33}N_8F_{14}O_2P_{2.33}Ru$: C, 47.7; H, 3.39; N, 8.9. Found: C, 47.8; H, 3.06; N, 8.6%.

$[Ru(Me_2bpy)(Me_4bpy)(dpq)](PF_6)_2\cdot 0.25HPF_6$. A mixture of $[Ru(Me_2bpy)(Me_4bpy)(CO)_2](PF_6)_2$ (50 mg, 0.059 mmol) and dpq (51 mg, 0.18 mmol) in 1,2-dimethoxyethane (20 mL) was sparged with nitrogen for 30 min. TMNO (12.5 mg, 0.18 mmol) was added and the mixture heated at reflux for 3 h. After cooling to room temperature, the supernatant was decanted and evaporated to dryness under reduced pressure. The crude product was purified by passage through a column of Sephadex LH20 (2.5 × 20 cm) with methanol as eluent. The central portion of the red band was collected and re-chromatographed. The red band was collected and evaporated to dryness under reduced pressure. Yield: 20 mg (32%). Anal. calculated for $C_{44}H_{40.25}N_8F_{13.5}O_2P_{2.25}Ru$: C, 47.7; H, 3.66; N, 10.1. Found: C, 47.7; H, 3.50; N, 9.5%.

$[Ru(Me_2bpy)(Me_4bpy)(dpb)](PF_6)_2\cdot 0.50HPF_6$. This salt was prepared in a similar manner to $[Ru(Me_2bpy)(Me_4bpy)(dpq)](PF_6)_2\cdot 0.25HPF_6$. $[Ru(Me_2bpy)(Me_4bpy)(CO)_2](PF_6)_2$ (73 mg, 0.087 mmol) was reacted with TMNO (30 mg, 0.42 mmol) in

the presence of dpb (87.5 mg, 0.27 mmol); purification was effected on a 2 × 40 cm column of Sephadex LH-20 (methanol eluent) and the purple band collected, and the solvent removed under reduced pressure. Yield: 25 mg (25%). Anal. Calculated for $C_{48}H_{42.5}N_8F_{15}O_2P_{2.5}Ru$: C, 48.3; H, 3.59; N, 9.4. Found: C, 48.3; H, 3.32; N, 8.8%.

[Ru(Me$_2$bpy){bpy(CO$_2$Et)$_2$}(Et$_2$dtc)]PF$_6$. [Ru(Me$_2$bpy){bpy(CO$_2$Et)$_2$}(CO)$_2$](PF$_6$)$_2$ (80 mg, 0.085 mmol) and potassium diethyldithiocarbamate (64 mg, 0.34 mmol) were combined with TMNO (12 mg, 0.17 mmol) in 1,2-dimethoxyethane (50 mL). The mixture was sparged with oxygen-scrubbed Ar for 1 h, then heated at reflux under an Ar atmosphere for 12 h. The deep purple solution was cooled to room temperature and the solvent removed under reduced pressure. The resulting residue was dissolved in water, absorbed on a 2.5 × 70 cm column of SP Sephadex C-25 cation exchanger, and eluted with a 0–100 mM KNO_3 gradient. The initial yellow and orange bands were discarded and the third (dark purple) band collected, concentrated under reduced pressure and extracted with dichloromethane (3 × 50 mL). The organic layers were combined, dried over anhydrous sodium sulfate, concentrated under reduced pressure, and added dropwise to swirling diethyl ether (100 mL). The resulting precipitate was collected on a medium porosity fritted glass funnel and re-eluted on a similar SP Sephadex C-25 column. The centre of the purple band was collected, and a purple precipitate obtained upon addition of saturated aqueous NH_4PF_6 solution (3 mL). This solid was dissolved in a minimum of acetonitrile and eluted with 3 : 1 (v/v) toluene–acetonitrile on a basic alumina column (2.5 × 30 cm). The centre of the purple band was collected. Slow evaporation of the acetonitrile over 12 h yielded the pure product as black microcrystals which were collected, washed with diethyl ether (5 × 5 mL) and dried overnight under vacuum at 50 °C. Yield: 18 mg (24%). ^{1}H NMR (acetone-d$_6$): δ 1.23 (m), 1.33 (t), 1.47 (t), 2.44 (s), 2.69 (s), 3.70 (m), 4.38 (q), 4.53 (q), 7.12 (d), 7.64 (d), 7.74 (m), 8.22 (d), 8.27 (d), 8.48 (s), 8.62 (s), 9.03 (s), 9.13 (s), 9.52 (d), 9.97 (d).

[Ru(Me$_2$bpy){bpy(CO$_2$Et)$_2$}(dpb)](PF$_6$)$_2$. A procedure similar to that for [Ru(Me$_2$bpy){bpy(CO$_2$Et)$_2$}(Et$_2$dtc)]PF$_6$ was followed. [Ru(Me$_2$bpy){bpy(CO$_2$Et)$_2$}(CO)$_2$](PF$_6$)$_2$ (53 mg, 0.049 mmol) was reacted with potassium diethyldithiocarbamate (45 g, 0.24 mmol) in the presence of TMNO (7 mg, 0.10 mmol) in 1,2-dimethoxyethane (150 mL) for 12 h. In this case the TMNO was pre-dissolved in 1,2-dimethoxyethane and diluted before addition so that an accurate weight could be used. Yield: 11 mg (22%).

[Ru(Me$_2$bpy){bpy(CO$_2$Et)$_2$}(SCN)$_2$]·H$_2$O. [Ru(Me$_2$bpy){bpy(CO$_2$Et)$_2$}(CO)$_2$](PF$_6$)$_2$ (0.44 g, 0.47 mmol) and potassium thiocyanate (0.22 g, 2.3 mmol) were combined with 2-methoxyethanol (100 mL) and the mixture deaerated by bubbling with Ar for 50 min. The mixture was heated to reflux forming a bright orange solution. Solid TMNO (74 mg, 0.99 mmol) was added in one portion to the hot solution and heating continued under Ar for an additional 5 h after which the solution was deep purple. The solution was cooled to room temperature and evaporated to dryness under vacuum. Dichloromethane (5 mL) was added to the residue. The mixture was sonicated for 10 min and filtered. Addition of diethyl ether (150 mL) to the filtrate yielded the crude product as a purple solid. The crude material was purified by column chromatography on an alumina support (15 cm length; 4 : 1 v/v toluene–acetonitrile eluent) and then silica gel (15 cm; methanol eluent). Yield: 0.16 g, 42%. ^{1}H NMR (dichloromethane-d$_2$): δ 1.37 (t, 3H), 1.51 (t, 3H), 2.42 (s, 3H), 2.68 (s, 3H), 4.42 (q, 2H), 4.55 (q, 2H), 6.86 (d, 1H), 7.18 (d, 1H), 7.58 (m, 2H), 7.78 (d, 1H), 7.93 (s, 1H), 8.07 (s, 1H), 8.21 (d, 1H), 8.71 (s, 1H), 8.86 (s, 1H), 9.29 (d, 1H), 9.72 (d, 1H). IR (KBr): ν_{CN} = 2100, ν_{CO} = 1723 cm^{-1}. Anal. calculated for $C_{30}H_{30}N_6O_5RuS_2$: C, 50.1; H, 4.21; N, 11.1. Found: C, 50.1; H, 4.22; N, 11.4%.

[Ru(bpy){bpy(CO$_2$Et)$_2$}(SCN)$_2$]. This complex was synthesised in an analogous manner to [Ru(Me$_2$bpy){bpy(CO$_2$Et)$_2$}(SCN)$_2$]·H$_2$O. ^{1}H NMR (dichloromethane-d$_2$): δ 1.39 (t, 3H), 1.51 (t, 3H), 4.40 (q, 2H), 4.54 (q, 2H), 7.05 (dd, 1H), 7.40 (d, 1H), 7.58 (d, 1H), 7.75 (m, 3H), 8.10 (m, 2H), 8.25 (m, 2H), 8.72 (s, 1H), 8.79 (s, 1H), 9.49 (d, 1H), 9.71 (d, 1H). Anal. calculated for $C_{28}H_{26}N_6O_4RuS_2$: C, 49.0; H, 3.82; N, 12.2. Found: C, 49.9; H, 3.61; N, 12.1%.

[Ru(Me$_4$bpy){bpy(CO$_2$Et)$_2$}(SCN)$_2$]·H$_2$O. This complex was prepared in an analogous manner to [Ru(Me$_2$bpy){bpy(CO$_2$Et)$_2$}(SCN)$_2$]·H$_2$O and [Ru(bpy){bpy(CO$_2$Et)$_2$}(SCN)$_2$]. ^{1}H NMR (dichloromethane-d$_2$): δ 1.36 (t, 3H), 1.48 (t, 3H), 1.95 (s, 3H), 2.30 (s, 3H), 2.49 (s, 3H), 2.55 (s, 3H), 4.40 (q, 2H), 4.53 (q, 2H), 6.94 (s, 1H), 7.52 (d, 1H), 7.72 (d, 1H), 7.81 (s, 1H), 7.95 (s, 1H), 8.20 (d, 1H), 8.70 (s, 1H), 8.84 (s, 1H), 9.09 (s, 1H), 9.70 (d, 1H). Anal. calculated for $C_{32}H_{34}N_6O_5RuS_2$: C, 51.4; H, 4.58; N, 11.2. Found: C, 51.4; H, 4.61; N, 11.1%.

Hydrolysis of ester complexes

Hydrolysis was achieved by adaption of a literature procedure.[107] The ester complex (25–50 mg) was dissolved in methanol (10–15 mL) and the solution stirred while five drops of a 50% (by weight) aqueous solution of NaOH were added. The reaction was allowed to stir overnight in the dark. Water (4 mL) was added to the solution and the methanol removed under reduced pressure. The aqueous solution was acidified to pH 2.5 by addition of 1 M perchloric acid, resulting in the immediate precipitation of the hydrolysed complex. The precipitate was collected by vacuum filtration and washed with slightly acidic water, then a small amount of cold water, and finally copiously with diethyl ether. To remove the last trace of water, the solids were dried under vacuum at 70 °C overnight.

Results

Syntheses

The syntheses of the tris(heteroleptic)ruthenium(II) complexes were carried out as previously reported.[44,46] Modifications were made to the procedures for complexes involving the potentially bridging ligands 2,3-bis(2-pyridyl)pyrazine (dpp), 2,3-bis(2-pyridyl)quinoxaline (dpq), and 2,3-bis(2-pyridyl)benzoquinoxaline (dpb) to avoid the formation of dinuclear species. The changes made related to variations in stoichiometries and concentrations, orders of addition, and purification procedures. The second step in the synthetic sequence to produce complexes of the type [Ru(BL)(CO)$_2$(O$_3$SCF$_3$)$_2$] {BL = dpp, dpq or dpb} was carried out in excess trifluoromethanesulfonic acid. With potential bridging ligands, protonation of the BL ligands occurred. The protonated complexes did react in the next step, but gave products in sharply reduced yields. Attempts to deprotonate the coordinated ligands led to decomposition of the complexes, especially in reactions involving the esterified ligand bpy(CO$_2$Et)$_2$, where hydrolysis may occur. Alternative routes are addressed elsewhere.[44]

The synthesis of heteroleptic thiocyanato-containing complexes has recently been reported.[109] A complicating factor in the coordination chemistry is possible linkage isomerism involving the thiocyanato ligand. However, as described by Kohle *et al.*[77] and others,[110,111] a combination of ^{1}H NMR and infrared spectroscopy were used to confirm that only the N-bound isomer was present in the final purified samples.

Electrochemistry and UV-visible spectroscopy

Table 1 summarises the cyclic voltammetry data associated with the tris(heteroleptic) complexes, and Table 2 electrochemical

Table 1 Reduction potentials[a]

Complex	$E_{½}^{III/II}$/V	$E_{½}^{0/-}$/V	$E_{½}^{2-/-}$/V	$E_{½}^{2-/3-}$/V
$[Ru(Me_2bpy)(Me_4bpy)(dpp)]^{2+}$	+1.26	−1.09	−1.61	−1.98
$[Ru(Me_2bpy)(Me_4bpy)(dpq)]^{2+}$	+1.28	−0.83	−1.54	−1.82
$[Ru(Me_2bpy)(Me_4bpy)(dpb)]^{2+}$	+1.29	−0.67	−1.35	−1.79
$[Ru(Me_2bpy)\{bpy(CO_2Et)_2\}(dpp)]^{2+}$	+1.45	−0.96	−1.19	−1.66
$[Ru(Me_2bpy)\{bpy(CO_2Et)_2\}(dpq)]^{2+}$	+1.47	−0.75	−1.12	−1.62
$[Ru(Me_2bpy)\{bpy(CO_2Et)_2\}(dpb)]^{2+}$	+1.47	−0.59	−1.09	−1.47
$[Ru(Me_2bpy)\{bpy(CO_2Et)_2\}(Et_2dtc)]^{+}$	+0.62	−1.25	−1.45	—
$[Ru\{bpy(CO_2Et)_2\}(dpb)(Et_2dtc)]^{+}$	+0.79	−0.76	−1.23	−1.73
$[Ru(bpy)\{bpy(CO_2Et)_2\}(SCN)_2]$	+0.81[b]	−1.13	−1.60[c]	—
$[Ru(Me_2bpy)\{bpy(CO_2Et)_2\}(SCN)_2]$	+0.73	−1.19	−1.67[d]	—
$[Ru(Me_4bpy)\{bpy(CO_2Et)_2\}(SCN)_2]$	+0.72	−1.18	—	—

[a] *Versus* SSCE in acetonitrile with 0.1 M tetra-*n*-butylammonium hexafluorophosphate at room temperature. [b] Additional reversible wave at $E_{p,a}$ = +1.23 V. [c] Slightly irreversible. [d] $E_{p,c}$ value for irreversible reduction.

Table 2 Reduction potentials for homoleptic and bis(heteroleptic) complexes[a]

Complex	$E_{½}^{III/II}$/V	$E_{½}^{0/-}$/V	$E_{½}^{2-/-}$/V	$E_{½}^{2-/3-}$/V	Ref.
$[Ru(bpy)_3]^{2+}$ [a]	+1.29	−1.33	−1.52	−1.78	[c]
$[Ru(bpy)_3]^{2+}$ [b]	+1.24	−1.27	−1.46	−1.70	122
$[Ru(Me_2bpy)_3]^{2+}$ [a]	+1.12	−1.45	−1.63	—	115
$[Ru(Me_4bpy)_3]^{2+}$ [a]	+1.06	−1.49	−1.70	−1.99	123
$[Ru\{bpy(CO_2Et)_2\}_3]^{2+}$ [b]	+1.55	−0.89	−1.01	−1.19	122
$[Ru(dpp)_3]^{2+}$ [a]	+1.68	−0.95	−1.12	−1.39	[c]
$[Ru(dpq)_3]^{2+}$ [a]	+1.65	−0.62	−0.81	−1.08	[c]
$[Ru(dpb)_3]^{2+}$ [a]	+1.70	−0.47	−0.65	−0.88	[c]
$[Ru(bpy)_2(Me_2bpy)_2]^{2+}$ [a]	+1.24	−1.36	−1.56	−1.82	115
$[Ru(Me_2bpy)_2(bpy)]^{2+}$ [a]	+1.18	−1.43	−1.64	−1.87	115
$[Ru(Me_2bpy)_2(py)_2]^{2+}$ [a]	+1.20	−1.46	−1.65	—	115
$[Ru(bpy)_2\{bpy(CO_2Et)_2\}]^{2+}$ [b]	+1.54	−0.93	−1.36	−1.56	122

[a] *Versus* SSCE in acetonitrile with 0.1 M tetra-*n*-butylammonium hexafluorophosphate at room temperature. [b] In DMF solution with 0.1 M tetra-*n*-butylammonium hexafluorophosphate at room temperature. [c] This work.

parameters for a number of homoleptic and bis(heteroleptic) complexes. Known substituent effects and the roles of electron-donating (*e.g.* methyl) and electron-withdrawing (*e.g.* carboxylic ester) groups[44,63] were used in assigning the ligand reductions in the tables. The ease of reduction from most negative to least negative potentials are in the order $Me_4bpy > Me_2bpy > bpy > bpy(CO_2Et)_2 \sim dpp > dpq > dpb$ (Fig. 1).

In all cases except the thiocyanato and chloro complexes, redox couples were chemically reversible and electrochemically reversible or quasi-reversible. The Ru(III) forms of thiocyanato complexes were unstable when the Ru(III/II) couples had $E_{½}$ >1, presumably with formation of thiocyanogen as observed in related complexes.[111] The second ligand-based reductions were also slightly or completely irreversible. This irreversibility may involve loss of anionic thiocyanate as found for reductions of halo complexes of ruthenium(II).[112]

Figs. 2–4 show absorption spectra (acetonitrile solution) for $[Ru(Me_4bpy)(Me_2bpy)(BL)]^{2+}$, $[Ru(Me_2bpy)\{bpy(CO_2Et)_2\}(BL)]^{2+}$ and $[Ru\{bpy(CO_2Et)_2\}(Et_2dtc)(pp)]^{+}$ {where BL = dpp, dpq and dpb; pp = Me_2bpy, dpb}, and of $[Ru(bpy)_3]^{2+}$ for comparison. Band assignments were made as described in the Discussion. For $[Ru(Me_2bpy)\{bpy(CO_2Et)_2\}(dpp)]^{2+}$, the assignment of the site of the first reduction and acceptor ligand for the lowest-energy charge transfer transition – either $bpy(CO_2Et)_2$ or dpp – is ambiguous. The ester ligand is predicted[44] based on the Lever parameters,[113] an assignment that has subsequently been confirmed by time-resolved resonance Raman (TR^3) spectra.[114]

Dye-derivatized semiconductor cells

Fig. 5 shows absorbance spectra for $[Ru\{bpy(CO_2Et)_2\}(pp)(SCN)_2]$ {pp = bpy, Me_2bpy, and Me_4bpy}. The spectra are related with small red shifts occurring in the lowest energy MLCT band in the order pp = bpy < Me_2bpy < Me_4bpy. The molar absorption coefficients are similar (Table 3). These complexes were hydrolysed and adsorbed onto titanium dioxide-coated transparent tin-doped indium oxide electrodes as described in the Experimental section. The following photocurrent producing reactions occurred when the cells were assembled (Scheme 1).

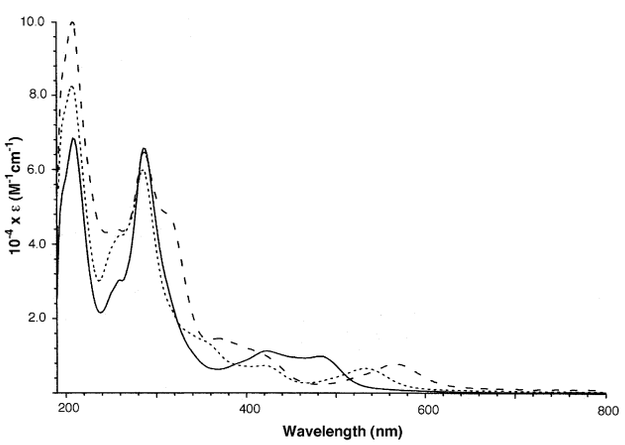

Fig. 2 UV-Visible absorbance spectra for the series $[Ru(Me_4bpy)(Me_2bpy)(BL)]^{2+}$ in acetonitrile solution at room temperature {BL = dpb ---; dpq • • •; dpp ——}.

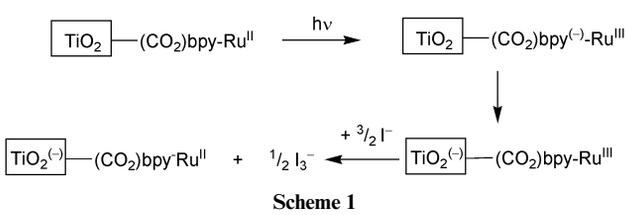

Scheme 1

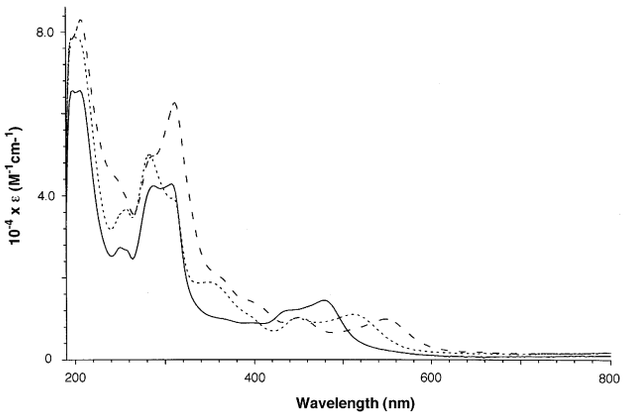

Fig. 3 UV-Visible absorbance spectra for the series $[Ru(Me_2bpy)\{bpy(CO_2Et)_2\}(BL)]^{2+}$ in acetonitrile solution at room temperature {BL = dpb ---; dpq · · ·; dpp ——}.

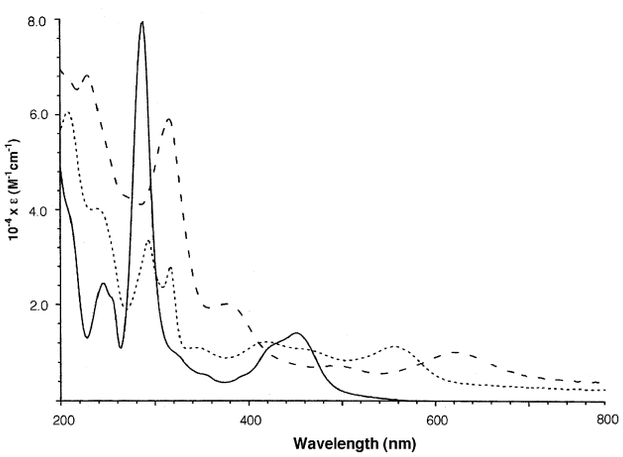

Fig. 4 UV-Visible absorbance spectra for $[Ru\{bpy(CO_2Et)_2\}(Et_2dtc)(dpb)]^+$ (---) and $[Ru\{bpy(CO_2Et)_2\}(Et_2dtc)(Me_2bpy)]^+$ (· · ·) in acetonitrile solution at room temperature. The spectrum of $[Ru(bpy)_3]^{2+}$ is shown for comparison (——).

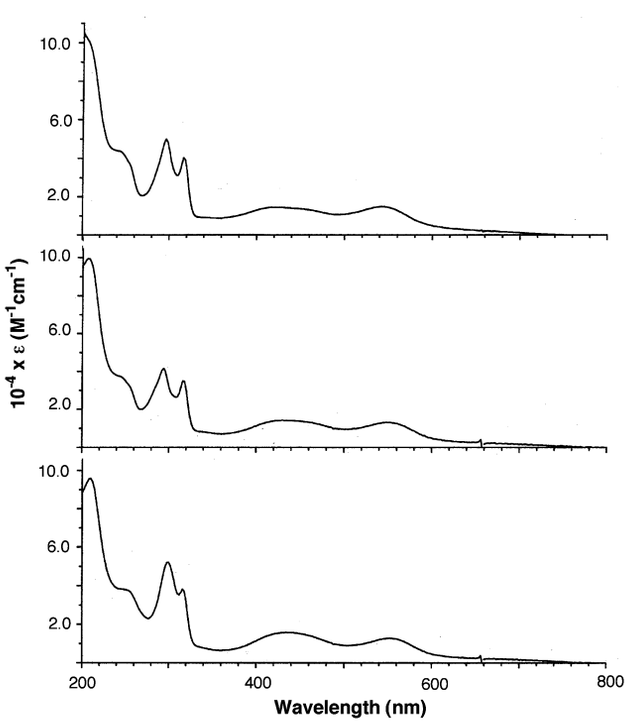

Fig. 5 UV-Visible absorbance spectra for the series $[Ru\{bpy(CO_2Et)_2\}(pp)(SCN)_2]$ {pp = bpy (top), Me_2bpy (middle) and Me_4bpy (bottom)} in acetonitrile solution at room temperature.

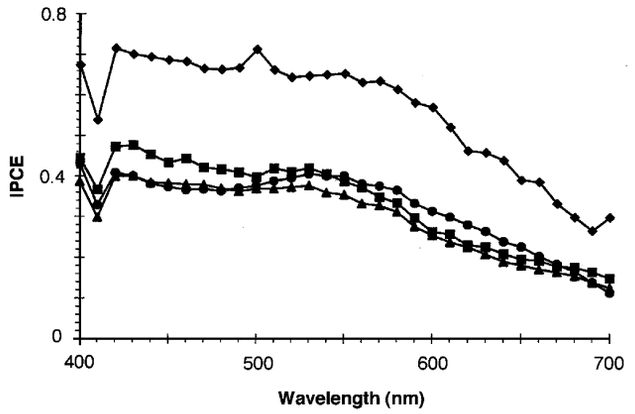

Fig. 6 Photo-current action spectra for TiO_2 films coated with $[Ru\{bpy(CO_2H)_2\}_2(SCN)_2]$ (●), $[Ru(Me_4bpy)\{bpy(CO_2H)_2\}(SCN)_2]$ (■), $[Ru(Me_2bpy)\{bpy(CO_2H)_2\}(SCN)_2]$ (▲), and $[Ru(bpy)\{bpy(CO_2H)_2\}(SCN)_2]$ (◆). Spectra were acquired in a two-electrode cell containing a solution of 0.5 M NaI and 0.05 M I_2 in propylene carbonate solution; IPCE values are corrected for light intensity losses due to absorption and reflection by the glass support.

An IPCE–wavelength plot is shown in Fig. 6, and absorbance spectra for adsorbed $[Ru\{bpy(CO_2H)_2\}_2(SCN)_2]^{n+}$ and $[Ru(bpy)\{bpy(CO_2H)_2\}(SCN)_2]^{n+}$ in Fig. 7, along with a light-harvesting efficiency (LHE)–wavelength plot.

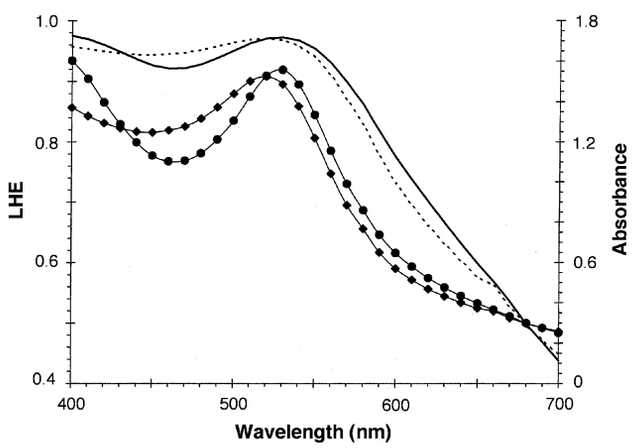

Fig. 7 Plot of light harvesting efficiencies (LHE) for $[Ru\{bpy(CO_2H)_2\}_2(SCN)_2]$ (——) and $[Ru(bpy)\{bpy(CO_2H)_2\}(SCN)_2]$ (· · ·) and visible absorption spectra for the homoleptic (●) and heteroleptic (◆) complexes. The spectra were acquired on bare TiO_2 derivatised electrodes.

Discussion

Electrochemistry

Ligand-based reduction potentials are increasingly negative in the order dpb > dpq > dpp ~ $bpy(CO_2Et)_2$ > bpy > Me_2bpy > Me_4bpy. This is the ordering for the first ligand reduction potentials for the homoleptic complexes $[Ru(pp)_3]^{2+}$ (Table 2). The order is maintained in mixed-chelate complexes (Table 1). For example, the first ligand reduction in $[Ru(bpy)_2\{bpy(CO_2Et)_2\}]^{2+}$ occurs at −0.93 V (*vs.* SSCE) and near −0.89 V in $[Ru\{bpy(CO_2Et)_2\}_3]^{2+}$. The first reduction in $[Ru(bpy)_3]^{2+}$ occurs at −1.33 V. The second reduction in the mixed-chelate complex occurs at −1.36 V, near the second reduction −1.52 V in $[Ru(bpy)_3]^{2+}$, but different from −1.01 V in $[Ru\{bpy(CO_2Et)_2\}_3]^{2+}$. There are additional examples in Table 2. The first reduction in $[Ru(bpy)_2(Me_2bpy)]^{2+}$ is at −1.36 V compared to −1.33 V for $[Ru(bpy)_3]^{2+}$. The first reduction for $[Ru(Me_2bpy)_3]^{2+}$ is at −1.45 V and the second reduction of $[Ru(Me_2bpy)_2(bpy)]^{2+}$ at −1.64 V, which is within experimental error of the second reduction in $[Ru(Me_2bpy)_3]^{2+}$ at −1.63 V, compared to −1.52 V in $[Ru(bpy)_3]^{2+}$. These comparisons are limited to

Table 3 UV-Visible bands and assignments for complexes in CH_3CN

Complex	λ_{max}/nm	$10^{-4}\ \varepsilon$/M^{-1} cm^{-1}	Assignment
$[Ru(Me_2bpy)(Me_4bpy)(dpp)]^{2+}$	200	5.57	$\pi \longrightarrow \pi^*$ Me_2bpy, Me_4bpy
	208	6.85	$\pi \longrightarrow \pi^*$ dpp
	259	3.00	$d\pi \longrightarrow \pi_2^*$ Me_2bpy, Me_4bpy, dpp
	286	6.57	$\pi \longrightarrow \pi_1^*$ Me_2bpy, Me_4bpy, dpp
	422	1.13	$d\pi \longrightarrow \pi_1^*$ Me_2bpy, Me_4bpy
	482	0.99	$d\pi \longrightarrow \pi_1^*$ dpp
$[Ru(Me_2bpy)(Me_4bpy)(dpq)]^{2+}$	198	7.44	$\pi \longrightarrow \pi^*$ Me_2bpy, Me_4bpy
	208	8.25	$\pi \longrightarrow \pi^*$ dpq
	260	4.24	$d\pi \longrightarrow \pi_2^*$ Me_2bpy, Me_4bpy
	286	5.99	$\pi \longrightarrow \pi_2^*$ Me_2bpy, Me_4bpy
	316	2.28	$\pi \longrightarrow \pi^*$ dpq
	350	1.43	$d\pi \longrightarrow \pi_2^*$ dpq
	422	0.73	$d\pi \longrightarrow \pi_1^*$ Me_2bpy, Me_4bpy
	534	0.67	$d\pi \longrightarrow \pi_1^*$ dpq
$[Ru(Me_2bpy)(Me_4bpy)(dpb)]^{2+}$	200	9.00	$\pi \longrightarrow \pi^*$ Me_2bpy, Me_4bpy
	208	10.00	$\pi \longrightarrow \pi^*$ dpb
	258	4.39	$d\pi \longrightarrow \pi_2^*$ Me_2bpy, Me_4bpy
	286	6.47	$\pi \longrightarrow \pi^*$ Me_2bpy, Me_4bpy
	318	4.64	$\pi \longrightarrow \pi^*$ dpb
	368	1.46	$d\pi \longrightarrow \pi_2^*$ dpb
	422	1.00	$d\pi \longrightarrow \pi_1^*$ Me_2bpy, Me_4bpy
	564	0.78	$d\pi \longrightarrow \pi_1^*$ dpb
$[Ru(Me_2bpy)\{bpy(CO_2Et)_2\}(dpp)]^{2+}$	200	6.51	$\pi \longrightarrow \pi^*$ Me_2bpy
	208	6.50	$\pi \longrightarrow \pi^*$ $bpy(CO_2Et)_2$
	248	2.72	$d\pi \longrightarrow \pi^*$ Me_2bpy, $bpy(CO_2Et)_2$, dpp
	258	2.66	$d\pi \longrightarrow \pi_2^*$ $bpy(CO_2Et)_2$, dpp
	288	4.24	$\pi \longrightarrow \pi^*$ Me_2bpy
	308	4.29	$\pi \longrightarrow \pi^*$ $bpy(CO_2Et)_2$, dpp
	444	1.21	$d\pi \longrightarrow \pi_1^*$ Me_2bpy
	480	1.43	$d\pi \longrightarrow \pi_1^*$ $bpy(CO_2Et)_2$, dpp
$[Ru(Me_2bpy)\{bpy(CO_2Et)_2\}(dpq)]^{2+}$	200	7.88	$\pi \longrightarrow \pi^*$ Me_2bpy
	209	7.59	$\pi \longrightarrow \pi^*$ $bpy(CO_2Et)_2$
	250	3.54	$d\pi \longrightarrow \pi_2^*$ $bpy(CO_2Et)_2$, dpq
	258	3.68	$d\pi \longrightarrow \pi^*$ $bpy(CO_2Et)_2$, dpq
	282	5.00	$\pi \longrightarrow \pi^*$ $bpy(CO_2Et)_2$
	310	3.94	$d\pi \longrightarrow \pi^*$ Me_2bpy
	448	1.01	$d\pi \longrightarrow \pi_1^*$ $bpy(CO_2Et)_2$
	510	1.10	$d\pi \longrightarrow \pi_1^*$ dpq
$[Ru(Me_2bpy)\{bpy(CO_2Et)_2\}(dpb)]^{2+}$	198	7.85	$\pi \longrightarrow \pi^*$ Me_2bpy
	206	8.30	$\pi \longrightarrow \pi^*$ $bpy(CO_2Et)_2$
	244	4.48	$d\pi \longrightarrow \pi^*$ $bpy(CO_2Et)_2$
	258	3.91	$d\pi \longrightarrow \pi_2^*$ dpb
	284	4.94	$\pi \longrightarrow \pi_1^*$ Me_2bpy
	312	6.26	$\pi \longrightarrow \pi^*$ $bpy(CO_2Et)_2$, dpb
	352	2.16	$d\pi \longrightarrow \pi_1^*$ Me_2bpy
	392	1.45	$d\pi \longrightarrow \pi_1^*$ Me_2bpy
	448	1.02	$d\pi \longrightarrow \pi_1^*$ $bpy(CO_2Et)_2$
	548	0.99	$d\pi \longrightarrow \pi_1^*$ dpb
$[Ru(Me_2bpy)\{bpy(CO_2Et)_2\}(Et_2dtc)]^{+}$	208	6.06	$\pi \longrightarrow \pi_2^*$ Me_2bpy
	238	4.02	$\pi \longrightarrow \pi_2^*$ $bpy(CO_2Et)_2$
	294	3.34	$\pi \longrightarrow \pi_1^*$ Me_2bpy
	316	2.78	$\pi \longrightarrow \pi_1^*$ $bpy(CO_2Et)_2$
	344	1.10	$d\pi \longrightarrow \pi_2^*$ $bpy(CO_2Et)_2$
	418	1.21	$d\pi \longrightarrow \pi_2^*$ Me_2bpy
	454	1.08	$d\pi \longrightarrow \pi_1^*$ Me_2bpy
	556	1.15	$d\pi \longrightarrow \pi_1^*$ $bpy(CO_2Et)_2$
$[Ru\{bpy(CO_2Et)_2\}(dpb)(Et_2dtc)]^{+}$	208	6.78[a]	$\pi \longrightarrow \pi^*$ dpb
	228	6.82	$\pi \longrightarrow \pi^*$ $bpy(CO_2Et)_2$
	275	4.21	$d\pi \longrightarrow \pi^*$ dpb
	316	5.91	$\pi \longrightarrow \pi^*$ $bpy(CO_2Et)_2$
	376	2.01	$\pi \longrightarrow \pi^*$ dpb
	490	0.73	$d\pi \longrightarrow \pi_1^*$ $bpy(CO_2Et)_2$
	620	1.01	$d\pi \longrightarrow \pi_1^*$ dpb
$[Ru(bpy)\{bpy(CO_2Et)_2\}(SCN)_2]$	206	10.0	
	240	4.39	
	296	5.00	
	316	4.02	
	422	1.45	
	542	1.48	

Table 3 (*Contd.*)

Complex	λ_{max}/nm	$10^{-4}\,\varepsilon$/M^{-1} cm^{-1}	Assignment
[Ru(Me$_2$bpy){bpy(CO$_2$Et)$_2$}(SCN)$_2$]	206	9.95	
	242	3.76	
	294	4.16	
	316	3.49	
	434	1.42	
	550	1.32	
[Ru(Me$_4$bpy){bpy(CO$_2$Et)$_2$}(SCN)$_2$]	210	9.57	
	246	3.82	
	300	5.20	
	316	3.80	
	428	1.58	
	554	1.28	

[a] Estimation of shoulder.

structurally related complexes of the same charge type. Ligand-based potentials respond to electron content at the metal (as measured by the Ru$^{III/II}$ couple). The first ligand reduction in [Ru(Me$_2$bpy)$_2$(bpy)]$^{2+}$ is shifted negatively by ~50 mV relative to [Ru(bpy)$_3$]$^{2+}$ because of electron donation to Ru(II) by the methyl-substituted bpy relative to bpy, which enhances dπ $\longrightarrow$ π*(bpy) electron donation.

There is an additional trend in these data. Within the two series [Ru(Me$_2$bpy){bpy(CO$_2$Et)$_2$}(BL)]$^{2+}$ and [Ru(Me$_2$bpy)-(Me$_4$bpy)(BL)]$^{2+}$ {BL = dpp, dpq and dpb} the second ligand reductions, based on bpy(CO$_2$Et)$_2$ and Me$_2$bpy respectively, occur at more positive potentials than expected. This is a result of delocalisation of the first electron over a more extended π* framework, which decreases electron–electron repulsion upon addition of the second electron.

Absorbance spectra

The intense visible absorption bands arise from MLCT transitions from the singlet ground state to largely singlet excited states.[31,40] The analogous transitions to the corresponding triplet excited states appear as overlapping bands of low absorptivity at lower energy. Metal-centred dd bands (dπ $\longrightarrow$ dσ*) are Laporte forbidden, of low intensity and masked by the MLCT bands. Ligand-centred π $\longrightarrow$ π* bands appear in the UV. The assignments of the lowest-energy MLCT absorptions can be made on the basis of $\Delta E_{1/2}$ values, the difference in the reduction potentials for the Ru$^{III/II}$ and pp$^{0/-}$ couples (pp is a bidentate polypyridyl ligand).[115–119] This procedure was used to assign the acceptor ligands in MLCT transitions to the lowest π* levels of the remaining ligands. Where equivocal, distinction between MLCT and π $\longrightarrow$ π* bands was made by appearance or non-appearance of a solvent dependence since π $\longrightarrow$ π* bands are only slightly solvent dependent.[120] Where two MLCT bands were observed to a single ligand, the energy difference between the lowest and second lowest π* ligand levels could be determined.

The absorbance spectrum of [Ru(Me$_2$bpy){bpy(CO$_2$Et)$_2$}-(Et$_2$dtc)]$^+$ is provided as ESI (Fig. S1, shown with the abscissa linear in energy). Based on the first reduction potentials of [Ru(Me$_2$bpy)$_3$]$^{2+}$ and [Ru{bpy(CO$_2$Et)$_2$}$_3$]$^{2+}$ in Tables 1 and 2, the ester-functionalised ligand is easier to reduce, and is the acceptor for the lowest MLCT band at 18000 cm^{-1}. A band at 23900 cm^{-1} and shoulder at ~22000 cm^{-1} are MLCT bands to the Me$_2$bpy ligand. The high absorptivities of bands between 50000 and 30000 cm^{-1} are consistent with their assignment as π $\longrightarrow$ π* transitions. The separation between bands at 48100 and 34000 cm^{-1} (~14000 cm^{-1}) is the same as for analogous bands in [Ru(Me$_2$bpy)$_3$]$^{2+}$, [Ru(Me$_2$bpy)(Me$_4$bpy)(BL)]$^{2+}$, and [Ru(Me$_2$-bpy){bpy(CO$_2$Et)$_2$}(BL)]$^{2+}$. The common factor is Me$_2$bpy as an acceptor and these bands can be assigned to π $\longrightarrow$ π_1* and π $\longrightarrow$ π_2* on Me$_2$bpy. Similarly, the bands at 42000 and 31600 cm^{-1} can be assigned to π $\longrightarrow$ π_1* and π $\longrightarrow$ π_2* on bpy(CO$_2$Et)$_2$ and the remaining band at 29100 cm^{-1} to dπ $\longrightarrow$ π_2*, the second MLCT transition to bpy(CO$_2$Et)$_2$. The energy differences between π_2* and π_1* derived from the MLCT bands and π $\longrightarrow$ π* bands for Me$_2$bpy are the same, as expected.

Designing black MLCT absorbers

In designing MLCT chromophores that absorb well into the visible, it is necessary to provide a low-lying π* acceptor ligand and/or stablise the Ru(III) site formed in the transition. The effect of an increasingly lower energy π* acceptor orbital was investigated in the series [Ru(Me$_2$bpy)(Me$_4$bpy)(BL)]$^{2+}$ {BL = dpp, dpq and dpb}. From Fig. 2 and Table 1, the lowest energy MLCT band shifts in concert with the change in the ligand-based reduction potential, with λ_{max} = 482, 534 and 564 nm, respectively. For the tail of the lowest energy band in [Ru-(Me$_2$bpy)(Me$_4$bpy)(dpb)]$^{2+}$ in the mid-600 nm range, ε is ~1000 M^{-1} cm^{-1}. Also notable in these spectra is the enhancement of the absorption in the high-energy visible region at 350–370 nm for BL = dpq and BL = dpb. This enhancement arises from higher energy MLCT bands to π_2* on the quinoxaline ligands. For the other polypyridyl ligands, these bands are masked by π $\longrightarrow$ π * bands in the UV.

The shift to the red creates a spectral hole in the mid-visible region near 460 nm. In order to "fill" this region of the spectrum required adding a ligand with an intermediate π* energy level. In the series [Ru(Me$_2$bpy){bpy(CO$_2$Et)$_2$}(BL)]$^{2+}$ the expected red shift was observed in the lowest-lying MLCT band for BL = dpp, dpq and dpb with λ_{max} = 489, 510, and 548 (Fig. 3). These complexes display nearly continuous absorption from the UV to the red edge of the MLCT bands, with no spectral holes. This trade of ligands does lead to a slight blue shift in the lowest energy MLCT band because of the inductive effect of bpy(CO$_2$Et)$_2$ on Ru(II).

In the final set of spectra (Fig. 4) for [Ru(Me$_2$bpy){bpy-(CO$_2$Et)$_2$}(Et$_2$dtc)]$^+$ and [Ru{bpy(CO$_2$Et)$_2$}(dpb)(Et$_2$dtc)]$^+$, the anionic bidentate ligand diethylcarbamate (Et$_2$dtc$^-$ anion) was added to stabilise Ru(III). In [Ru(Me$_2$bpy){bpy(CO$_2$Et)$_2$}-(Et$_2$dtc)]$^+$ the effect is to shift the lowest energy MLCT band to 620 nm with ε >1000 M^{-1} cm^{-1} even at 750 nm, and no spectral gaps.

Photoelectrochemistry

The chromophores [Ru{bpy(CO$_2$H)$_2$}(pp)(SCN)$_2$] {pp = bpy, Me$_2$bpy or Me$_4$bpy; bpy(CO$_2$H)$_2$ is 2,2′-bipyridine-4,4′-dicarboxylic acid, the hydrolysed form of bpy(CO$_2$Et)$_2$} are low-energy absorbers. Fig. 6 shows the photo-current action spectra of TiO$_2$ electrodes derivatised by adsorption of each of the complexes. Efficiencies in all three cases are comparable to that of [Ru{bpy(CO$_2$Et)$_2$}(SCN)$_2$]. In this series, [Ru(bpy)-

Table 4 Emission energies and lifetimes by transient absorption and emission in de-oxygenated acetonitrile solution at room temperature

Complex	λ_{max}^{em}/nm	E_{em}/cm^{-1}	τ_{em}/ns	$10^{-6}\,k_{em}$/s^{-1}	τ_{abs}/ns	$10^{-6}\,k_{abs}$/s^{-1}
$[Ru(Me_2bpy)(Me_4bpy)(dpp)]^{2+}$	714	14000	242	4.13	245	4.08
$[Ru(Me_2bpy)(Me_4bpy)(dpq)]^{2+}$	838	11900	325	3.08	322	3.11
$[Ru(Me_2bpy)\{bpy(CO_2Et)_2\}(dpp)]^{2+}$	676	14800	852	1.17	831	1.20
$[Ru(Me_2bpy)\{bpy(CO_2Et)_2\}(dpq)]^{2+}$	788	12700	40	25.0	39	25.6
$[Ru(Me_2bpy)\{bpy(CO_2Et)_2\}(dpb)]^{2+}$	1030	9710	—	—	106	9.43

$\{bpy(CO_2H)_2\}(SCN)_2]$ has the highest IPCE, although the light-harvesting efficiencies are comparable. This complex is slightly more absorbing to the red, and the slight absorbance gap in the blue is "filled in" because of the heteroleptic nature of the complex. The absorbance spectra are plotted on the same graph.

Excited-state properties

Emission spectra for the series $[Ru(Me_2bpy)\{bpy(CO_2Et)_2\}(BL)]^{2+}$ in acetonitrile at room temperature are shown in Fig. 8. Spectra for $[Ru(Me_2bpy)(Me_4bpy)(dpp)]^{2+}$ and $[Ru(Me_2bpy)(Me_4bpy)(dpq)]^{2+}$ under the same conditions are provided in the ESI (Fig. S2). Due to experimental limitations we have been unable to acquire the spectrum of $[Ru(Me_2bpy)(Me_4bpy)(dpb)]^{2+}$. The gaps in the data presented are due to incomplete overlap in reliable PMT response between the visible and NIR emission spectrometers used for the measurements. These data are summarised in Table 4 and expand upon our preliminary accounts.[63,121]

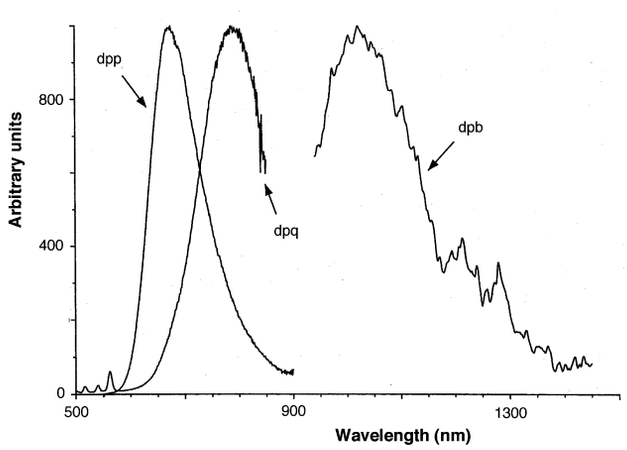

Fig. 8 Emission spectra for the series $[Ru(Me_2bpy)\{bpy(CO_2Et)_2\}(BL)]^{2+}$ in acetonitrile solution at room temperature {BL = dpb (right), dpq (center), and dpp (left)}. The spectra have been baseline-subtracted and normalized to a constant maximum intensity. The gaps in the data are a result of non-overlapping responses in the two luminescence instruments described in the Experimental.

Also included in Table 4 are excited state lifetime data as determined by transient absorbance measurements and, where possible, from time-resolved luminescence studies. In all cases in which the lifetimes could be determined by both methods, there was good agreement. This is important in showing the appropriateness of using transient absorbance measurements since this was the only method available for determining lifetimes for the NIR emitters.

The measured values reinforce the earlier observations showing the value of delocalised acceptor ligands in extending excited state lifetimes. These complexes are weak emitters and their lifetimes are dictated by nonradiative decay. Even though some of these complexes emit in the near-infrared, their lifetimes are on the nanosecond time-scale. This is especially dramatic in comparing $[Ru(Me_2bpy)(Me_4bpy)(BL)]^{2+}$ with BL = dpp and dpq: even though emission from the latter is red-shifted by 2100 cm^{-1}, the lifetime is extended from 242 to 325 ns.

There is no evidence for photochemical ligand loss from the complexes ($\Phi < 10^{-4}$), and temperature-dependent lifetime measurements on $[Ru(bpy)_2(dpp)]^{2+}$ reveal that dd states are not thermally accessible at room temperature and below. The data could be fitted to the expression,

$$\frac{1}{\tau} = \frac{k_0 + k_1\exp(-\Delta E/RT)}{1+\exp(-\Delta E/RT)}$$

The data and fit to the parameters $k_0 = 3.43 \times 10^6$ s^{-1}, $k_1 = 2.22 \times 10^8$ s^{-1}, and $\Delta E = 864$ cm^{-1} are given in the ESI (Fig. S3). These parameters are characteristic of decay from an upper MLCT state ~860 cm^{-1} above the low energy manifold of emitting state(s). Decay from this state contributes <2% to the overall decay of the excited state at room temperature.

Conclusions

A number of simple principles have emerged for designing the absorbance characteristics of polypyridyl complexes of ruthenium(II). Acceptor ligands with low-lying π* levels can be used to red shift the energy of the lowest MLCT bands. MLCT and π ⟶ π* bands originating on other ligands can be used to fill in the higher-energy regions of the spectrum. In addition, incorporation of anionic ligands or electron-donating ligands cause a red shift in MLCT bands compared to bpy. Electrochemical data can be used to predict the lowest energy ligand acceptor.

Attention to the design principles has led to the preparation of complexes which absorb appreciably in the near IR. The resulting complexes are free from complications caused by thermally accessible dd states. Even though their emission energies (and energy gaps) are at low energy in the near IR, the use of lowest lying, delocalised acceptor ligands provide lifetime enhancements (compared to bpy) that can be dramatic.

Acknowledgements

The authors wish to thank Dr Martin Devenney for acquiring the TR3 spectrum of $[Ru(Me_2bpy)\{bpy(CO_2Et)_2\}(dpp)](PF_6)_2$. Financial support from the Australian Research Council and the United States Department of Energy (Grant Number DE-FG02-96ER14607) is gratefully acknowledged. Travel between the two laboratories (G. F. S., P. A. A., J. A. T. and J. A. M.) has been supported by a United States National Science Foundation grant and the Australian Department of Industry, Science and Tourism within the Australian–US Bilateral Science and Technology Program.

References

1 S. L. Mecklenburg, K. A. Opperman, P. Y. Chen and T. J. Meyer, *J. Phys. Chem.*, 1996, **100**, 15145–15151.
2 K. A. Opperman, S. L. Mecklenburg and T. J. Meyer, *Inorg. Chem.*, 1994, **33**, 5295–5301.
3 S. L. Mecklenburg, B. M. Peek, J. R. Schoonover, D. G. McCafferty, C. G. Wall, B. W. Erickson and T. J. Meyer, *J. Am. Chem. Soc.*, 1993, **115**, 5479–5495.
4 L. Wallace and D. P. Rillema, *Inorg. Chem.*, 1993, **32**, 3836–3843.
5 S. L. Mecklenburg, D. G. McCafferty, J. R. Schoonover, B. M. Peek, B. W. Erickson and T. J. Meyer, *Inorg. Chem.*, 1994, **33**, 2974–2983.

6 B. M. Peek, G. T. Ross, S. W. Edwards, G. J. Meyer, T. J. Meyer and B. W. Erickson, *Int. J. Peptide Protein Res.*, 1991, **38**, 114–123.
7 M. R. Wasielewski, *Chem. Rev.*, 1992, **92**, 435–461.
8 D. Gust and T. A. Moore, *Science*, 1989, **244**, 35–41.
9 V. Balzani and F. Scandola, *Supramolecular Photochemistry*, Ellis Horwood, Chichester, 1991.
10 P. Belser, R. Dux, M. Baak, L. De Cola and V. Balzani, *Angew. Chem., Int. Ed. Engl.*, 1995, **34**, 595–598.
11 J.-P. Collin, S. Guillerez, J.-P. Sauvage, F. Barigelletti, L. De Cola, L. Flamigni and V. Balzani, *Inorg. Chem.*, 1991, **30**, 4230–4238.
12 J.-P. Sauvage, J.-P. Collin, J. C. Chambron, S. Guillerez, C. Coudret, V. Balzani, F. Barigelletti, L. De Cola and L. Flamigni, *Chem. Rev.*, 1994, **94**, 993–1019.
13 F. Scandola and V. Balzani, *J. Chem. Educ.*, 1983, **60**, 814–823.
14 J. D. Peterson, W. R. Murphy, R. Sahai, K. J. Brewer and R. R. Ruminski, *Coord. Chem. Rev.*, 1985, **64**, 261–272.
15 C. Creutz, M. Chou, T. L. Netzel, M. Okumura and N. Sutin, *J. Am. Chem. Soc.*, 1980, **102**, 1309–1319.
16 E. J. Lee and M. S. Wrighton, *J. Am. Chem. Soc.*, 1991, **114**, 8562–8564.
17 S. M. Baxter, W. E. Jones, E. Danielson, L. Worl, G. Strouse, J. Younathan and T. J. Meyer, *Coord. Chem. Rev.*, 1991, **111**, 47–71.
18 W. E. Jones, S. M. Baxter, G. F. Strouse and T. J. Meyer, *J. Am. Chem. Soc.*, 1993, **115**, 7363–7373.
19 L. A. Worl, G. F. Strouse, J. N. Younathan, S. M. Baxter and T. J. Meyer, *J. Am. Chem. Soc.*, 1990, **112**, 7571–7578.
20 J. N. Younathan, W. E. Jones and T. J. Meyer, *J. Phys. Chem.*, 1991, **95**, 488–492.
21 J. N. Younathan, S. F. McClanahan and T. J. Meyer, *Macromolecules*, 1989, **22**, 1048–1054.
22 G. F. Strouse, L. A. Worl, J. N. Younathan and T. J. Meyer, *J. Am. Chem. Soc.*, 1989, **111**, 9101–9102.
23 M. S. Wrighton, *J. Chem. Educ.*, 1983, **60**, 877–881.
24 M. K. Nazeeruddin, P. Pechy and M. Gratzel, *Chem. Commun.*, 1997, 1705–1706.
25 M. K. Nazeeruddin, A. Kay, I. Rodicio, R. Humphry-Baker, E. Müller, P. Liska, N. Vlachopolous and M. Gratzel, *J. Am. Chem. Soc.*, 1993, **115**, 6382–6390.
26 T. A. Heimer, F. N. Castellano and G. J. Meyer, *Inorg. Chem.*, 1994, **33**, 5741–5749.
27 T. A. Heimer, S. T. D'Arcangelis, F. Farzad, J. M. Stipkala and G. J. Meyer, *Inorg. Chem.*, 1996, **35**, 5319–5324.
28 T. A. Heimer, C. A. Bignozzi and G. J. Meyer, *J. Phys. Chem.*, 1993, **97**, 11987–11994.
29 R. Argazzi, C. A. Bignozzi, T. A. Heimer and G. J. Meyer, *Inorg. Chem.*, 1997, **36**, 2–3.
30 A. Hagfeldt and M. Grätzel, *Chem. Rev.*, 1995, **95**, 49–68.
31 E. M. Kober and T. J. Meyer, *Inorg. Chem.*, 1982, **21**, 3967–3977.
32 E. M. Kober and T. J. Meyer, *Inorg. Chem.*, 1983, **22**, 1614–1616.
33 D. R. Striplin and G. A. Crosby, *Chem. Phys. Lett.*, 1994, **221**, 426–430.
34 E. M. Kober, J. V. Caspar, B. P. Sullivan and T. J. Meyer, *Inorg. Chem.*, 1988, **27**, 4587–4598.
35 E. M. Kober, J. C. Marshall, W. J. Dressick, B. P. Sullivan, J. V. Caspar and T. J. Meyer, *Inorg. Chem.*, 1985, **24**, 2755–2763.
36 J. A. Baiano, D. L. Carlson, G. M. Wolosh, D. E. DeJesus, C. F. Knowles, E. G. Szabo and W. R. Murphy, *Inorg. Chem.*, 1990, **29**, 2327–2332.
37 R. R. Ruminski and R. T. Cambron, *Inorg. Chem.*, 1990, **29**, 1575–1578.
38 G. Tapolsky, R. Duesing and T. J. Meyer, *Inorg. Chem.*, 1990, **29**, 2285–2297.
39 E. M. Kober, B. P. Sullivan, W. J. Dressick, J. V. Caspar and T. J. Meyer, *J. Am. Chem. Soc.*, 1980, **102**, 7383–7385.
40 A. Juris, S. Barigelletti, S. Campagna, V. Balzani, P. Belser and A. von Zelewsky, *Coord. Chem. Rev.*, 1988, **84**, 85–277.
41 B. J. Coe, T. J. Meyer and P. S. White, *Inorg. Chem.*, 1995, **34**, 593.
42 B. J. Coe, D. W. Thompson, C. T. Culbertson, J. R. Schoonover and T. J. Meyer, *Inorg. Chem.*, 1995, **34**, 3385–3395.
43 B. J. Coe, T. J. Meyer and P. S. White, *Inorg. Chem.*, 1995, **34**, 3600–3609.
44 P. A. Anderson, G. B. Deacon, K. H. Haarmann, F. R. Keene, T. J. Meyer, D. A. Reitsma, B. W. Skelton, G. F. Strouse, N. C. Thomas, J. A. Treadway and A. H. White, *Inorg. Chem.*, 1995, **34**, 6145–6157.
45 B. P. Sullivan, D. J. Salmon and T. J. Meyer, *Inorg. Chem.*, 1978, **17**, 3334–3341.
46 G. F. Strouse, P. A. Anderson, J. R. Schoonover, T. J. Meyer and F. R. Keene, *Inorg. Chem.*, 1992, **31**, 3004–3006.
47 F. R. Keene, *Coord. Chem. Rev.*, 1997, **166**, 122–159.
48 J. V. Caspar and T. J. Meyer, *J. Am. Chem. Soc.*, 1983, **105**, 5583–5590.
49 B. Durham, J. V. Caspar, J. K. Nagle and T. J. Meyer, *J. Am. Chem. Soc.*, 1982, **104**, 4803–4810.
50 J. V. Caspar and T. J. Meyer, *Inorg. Chem.*, 1983, **22**, 2444–2453.
51 F. Barigelletti, L. De Cola and A. Juris, *Gazz. Chim. Ital.*, 1990, **120**, 545–551.
52 J. Van Houten and R. J. Watts, *J. Am. Chem. Soc.*, 1976, **98**, 4853–4858.
53 J. Van Houten and R. J. Watts, *Inorg. Chem.*, 1978, **17**, 3381–3385.
54 G. D. Hager and G. A. Crosby, *J. Am. Chem. Soc.*, 1975, **97**, 7031–7037.
55 R. Fasano and P. E. Hoggard, *Inorg. Chem.*, 1983, **22**, 566–567.
56 D. V. Pinnick and B. Durham, *Inorg. Chem.*, 1984, **23**, 1440–1445.
57 D. V. Pinnick and B. Durham, *Inorg. Chem.*, 1984, **23**, 3841–3842.
58 R. J. Crutchley and A. B. P. Lever, *Inorg. Chem.*, 1982, **21**, 2276–2282.
59 W. F. Wacholtz, R. A. Auerbach and R. H. Schmehl, *Inorg. Chem.*, 1986, **25**, 227–234.
60 L. J. Henderson, F. R. Fronczek and W. R. Cherry, *J. Am. Chem. Soc.*, 1984, **106**, 5876–5879.
61 M. Adelt, M. Devenney, T. J. Meyer, D. W. Thompson and J. A. Treadway, *Inorg. Chem.*, 1998, **37**, 2616–2617.
62 C. K. Jorgensen, *Absorption Spectra and Chemical Bonding in Complexes*, Pergammon, London, 1962.
63 P. A. Anderson, G. F. Strouse, J. A. Treadway, F. R. Keene and T. J. Meyer, *Inorg. Chem.*, 1994, **33**, 3863–3864.
64 E. Z. Jandrasics and F. R. Keene, *J. Chem. Soc., Dalton Trans.*, 1997, 153–159.
65 E. M. Kober, J. V. Caspar, R. S. Lumpkin and T. J. Meyer, *J. Phys. Chem.*, 1986, **90**, 3722–3734.
66 K. F. Freed, *Top. Curr. Chem.*, 1972, **31**, 105–139.
67 K. F. Freed and J. Jortner, *J. Chem. Phys.*, 1970, **52**, 6272–6291.
68 R. Englman and J. Jortner, *J. Mol. Phys.*, 1970, **18**, 145–164.
69 M. Bixon and J. Jortner, *J. Chem. Phys.*, 1968, **48**, 715–726.
70 J. P. Claude and T. J. Meyer, *J. Phys. Chem.*, 1995, **99**, 51–54.
71 J. V. Caspar, E. M. Kober, B. P. Sullivan and T. J. Meyer, *J. Am. Chem. Soc.*, 1982, **104**, 630–632.
72 J. V. Caspar, B. P. Sullivan, E. M. Kober and T. J. Meyer, *Chem. Phys. Lett.*, 1982, **91**, 91–95.
73 J. V. Caspar and T. J. Meyer, *J. Phys. Chem.*, 1983, **87**, 952–957.
74 R. Argazzi, C. A. Bignozzi, T. A. Heimer, F. N. Castellano and G. J. Meyer, *Inorg. Chem.*, 1994, **33**, 5741–5749.
75 R. Argazzi, C. A. Bignozzi, T. A. Heimer, F. N. Castellano and G. J. Meyer, *J. Am. Chem. Soc.*, 1995, **117**, 11815–11816.
76 S. M. Zakeeruddin, K. Nazeeruddin, R. Humphry-Baker and M. Gratzel, *Inorg. Chem.*, 1998, **37**, 5251–5259.
77 O. Kohle, S. Ruile and M. Grätzel, *Inorg. Chem.*, 1996, **35**, 4779–4787.
78 N. Vlachopoulos, P. Liska, J. Augustynski and M. Grätzel, *J. Am. Chem. Soc.*, 1988, **110**, 1216–1220.
79 B. O'Regan and M. Grätzel, *Nature*, 1991, **353**, 737–739.
80 G. Redmond and D. Fitzmaurice, *J. Phys. Chem.*, 1993, **97**, 1426–1430.
81 R. Eichberger and F. Willig, *Chem. Phys.*, 1990, **141**, 159–173.
82 G. K. Boschloo and A. Grossens, *J. Phys. Chem.*, 1996, **100**, 19494–19498.
83 J. N. Demas and D. G. Taylor, *Inorg. Chem.*, 1979, **18**, 3177–3179.
84 R. J. Watts, *J. Chem. Educ.*, 1983, **60**, 834–842.
85 F. E. Lytle and D. M. Hercules, *J. Am. Chem. Soc.*, 1969, **91**, 253–257.
86 P. A. Mabrouk and M. S. Wrighton, *Inorg. Chem.*, 1986, **25**, 526–531.
87 Y. J. Chang, X. Xu, T. Yabe, S.-C. Yu, D. R. Anderson, L. K. Orman and J. B. Hopkins, *J. Phys. Chem.*, 1990, **94**, 729–736.
88 P. G. Bradley, N. Kress, B. A. Hornberger, R. F. Dallinger and W. H. Woodruff, *J. Am. Chem. Soc.*, 1981, **103**, 7441–7556.
89 J. V. Caspar, T. D. Westmoreland, G. H. Allen, P. G. Bradley, T. J. Meyer and W. H. Woodruff, *J. Am. Chem. Soc.*, 1984, **106**, 3492–3500.
90 G. D. Danzer, J. A. Golus and J. R. Kincaid, *J. Am. Chem. Soc.*, 1993, **115**, 8643–8648.
91 W. E. Ford and M. Calvin, *Chem. Phys. Lett.*, 1980, **76**, 105–108.
92 H. Riesen, L. Wallace and E. Krausz, *Inorg. Chem.*, 1996, **35**, 6908–6909.
93 P. Chen, K. M. Omberg, D. A. Kavaliunas, J. A. Treadway, R. A. Palmer and T. J. Meyer, *Inorg. Chem.*, 1997, **36**, 954–955.
94 J. A. Treadway, B. Loeb, R. Lopez, P. A. Anderson, F. R. Keene and T. J. Meyer, *Inorg. Chem.*, 1996, **35**, 2242–2246.
95 E. M. Kober and T. J. Meyer, *Inorg. Chem.*, 1985, **24**, 106–108.
96 D. P. Strommen, T. K. Mallick, G. D. Danzer, R. S. Lumpkin and J. R. Kincaid, *J. Phys. Chem.*, 1990, **94**, 1357–1366.

97 J. V. Caspar, T. D. Westmoreland, G. H. Allen, P. G. Bradley, T. J. Meyer and W. H. Woodruff, *J. Am. Chem. Soc.*, 1984, **106**, 3492–3500.
98 D. P. Rillema, C. B. Blanton, R. J. Shaver, D. C. Jackman, M. Boldaji, S. Bundy, L. A. Worl and T. J. Meyer, *Inorg. Chem.*, 1992, **31**, 1600–1606.
99 B. O'Regan, J. Moser, M. Anderson and M. Grätzel, *J. Phys. Chem.*, 1990, **94**, 8720–8726.
100 R. Amadelli, R. Argazzi, C. A. Bignozzi and F. Scandola, *J. Am. Chem. Soc.*, 1990, **112**, 7099–7103.
101 R. Duesing, G. Tapolsky and T. J. Meyer, *J. Am. Chem. Soc.*, 1990, **112**, 5378–5379.
102 E. Danielson, personal communication.
103 D. W. Marquardt, *J. Soc. Ind. Appl. Math.*, 1963, **11**, 431–441.
104 E. E. Wegner and A. W. Adamson, *J. Am. Chem. Soc.*, 1966, **88**, 394–403.
105 H. A. Goodwin and F. Lions, *J. Am. Chem. Soc.*, 1959, **81**, 6415–6422.
106 A. Launikonis, P. A. Lay, A. W.-H. Mau, A. M. Sargeson and W. H. F. Sasse, *Aust. J. Chem.*, 1986, **39**, 1053–1062.
107 B. T. Patterson and F. R. Keene, *Aust. J. Chem.*, 1998, **51**, 999–1002.
108 B. T. Patterson and F. R. Keene, *Inorg. Chem.*, 1998, **37**, 645–650.
109 J. A. Treadway and T. J. Meyer, *Inorg. Chem.*, 1999, **38**, 2267–2278.
110 A. Golub, H. Kohler and V. V. Skopenko, *Chemistry of Pseudohalides*, Elsevier, Amsterdam, 1986.
111 A. A. Newman, *Chemistry and Biochemistry of Thiocyanic Acid and its Derivatives*, Academic Press, New York, 1975.
112 B. P. Sullivan, D. Conrad and T. J. Meyer, *Inorg. Chem.*, 1985, **24**, 3640–3645.
113 A. B. P. Lever, *Inorg. Chem.*, 1990, **29**, 1271–1285.
114 M. Devenney, personal communication.
115 H. B. Ross, M. Boldaji, D. P. Rillema, C. B. Blanton and R. P. White, *Inorg. Chem.*, 1989, **28**, 1013–1021.
116 A. Juris, S. Campagna, V. Balzani and G. Gremaud, *Inorg. Chem.*, 1988, **27**, 3652–3655.
117 D. P. Rillema, G. Allen, T. J. Meyer and D. Conrad, *Inorg. Chem.*, 1983, **22**, 1617–1622.
118 D. E. Morris, Y. Ohsawa, D. P. Segers, M. K. De Armond and K. W. Hanck, *Inorg. Chem.*, 1984, **23**, 3010–3017.
119 Y. Ohsawa, K. W. Hanck and M. K. De Armond, *J. Electroanal. Chem.*, 1984, **175**, 229–240.
120 P. Y. Chen, S. L. Mecklenburg and T. J. Meyer, *J. Phys. Chem.*, 1993, **97**, 13126–13131.
121 J. A. Treadway, G. F. Strouse, R. R. Ruminski and T. J. Meyer, *Inorg. Chem.*, 2001, **40**, 4508–4509.
122 C. M. Elliott and E. J. Hershenhart, *J. Am. Chem. Soc.*, 1982, **104**, 7519–7526.
123 C. M. Elliott, R. A. Freitag and D. D. Blaney, *J. Am. Chem. Soc.*, 1985, **107**, 4647–4655.